



Synthesis and electrochemical study of nanoporous Pd–Ag alloys for hydrogen sorption

Shuai Chen, Brian D. Adams, Aicheng Chen^{*,1}

Department of Chemistry, Lakehead University, 955 Oliver Road, Thunder Bay, Ontario P7B 5E1, Canada

ARTICLE INFO

Article history:

Received 9 August 2010
Received in revised form
21 September 2010
Accepted 21 September 2010
Available online 25 September 2010

Keywords:

Hydrogen purification
Hydrogen storage
Pd–Ag alloys
Nanoporous material
Hydrothermal method

ABSTRACT

We report on the synthesis of novel nanoporous Pd–Ag electrocatalysts using a facile hydrothermal method where the portion of Ag was varied from 0 to 40%. Scanning electron microscopy (SEM) was used to examine the morphologies of the prepared nanoporous materials. Energy dispersive X-ray spectroscopy (EDS), X-ray photoelectron spectroscopy (XPS) and inductively coupled plasma (ICP) were used to directly and indirectly characterize the composition of the formed Pd–Ag nanostructures. X-ray diffraction (XRD) analysis confirmed that the formed Pd–Ag nanomaterials were alloys with a face-centered cubic structure. Electrochemical methods were used to study the capacity and kinetics of hydrogen sorption into the nanoporous Pd and Pd–Ag alloys. The nanoporous Pd–Ag alloy with 20% silver possesses the highest capacity for the α phase hydrogen sorption, which is over 4 times higher than the pure nanoporous Pd. The combination of the enhanced α phase hydrogen sorption capacity and diminishing of the α - and β -phase transition makes the nanoporous Pd–Ag alloys promising for hydrogen selective membranes and hydrogen dissociation catalysts.

© 2010 Elsevier Ltd. All rights reserved.

1. Introduction

Hydrogen, because of its large combustion heat (287 kJ/mole) and its environmentally compatible by-product, water, is being extensively researched as an alternative to fossil fuels [1–4]. Storing hydrogen in a gas form or handling hydrogen in a liquid state at a critical low temperature (32.97 K) presents difficult challenges for its practical usage. Hydrogen storage alloys provide one of the best ways to store hydrogen compactly and safely as a consequence of the high stability of their hydride [5–11]. Driven by the need to develop hydrogen absorption materials, studies on the interaction between metals and hydrogen have become increasingly important. Electrochemical study provides a feasible approach to determine the thermodynamic and kinetic parameters of hydrogen sorption, which is important for the development of new materials for hydrogen storage. Most studies have been focused on finding the optimal properties of the metallic materials in terms of fast hydriding/dehydriding kinetics, large hydrogen-uptake capacity, high cycle stability, and reasonable production costs [12–14]. Poor reversibility and slow kinetics are the main problems of many metal hydride systems such as MgH_2 and NaAlH_4 [3].

Palladium and its alloys are classical materials for storing hydrogen above room temperature and show fast adsorption/absorption rates [13,15–17]. The palladium/hydrogen system has been intensively investigated both in the gas phase and under electrochemical conditions, due to its potential applications in hydrogen storage, metal-hydride batteries and hydrogen purification [18–21]. However, the use of Pd as the sole metal hydride for hydrogen storage is not practical because of its high cost and the hydrogen embrittlement caused by the phase transition from α to β in pure palladium [22]. Pd-based alloys, on the other hand, offer a class of attractive materials for studying metal hydrides because of the high solubility and permeability of hydrogen compared to pure Pd as well as the reduced cost if cheaper metals are added [23–29]. Great attention has been paid to nanostructured materials because of their high surface areas and significantly different properties compared to conventional materials with coarse grains [30–33]. For instance, recent study has revealed that the electrochemical response of hydrogen at Pd is critically dependent on the size and structure of the Pd surface [34]. The analytical response can be easily tailored in favor of either H_{ad} oxidation or H_{ab} oxidation by nanoscale tuning the coverage of Pd on Au nanoparticles. Nanostructured materials show distinct advantages in their hydrogen uptake characteristics compared with their bulk counterparts. Rapid hydrogen diffusion has been reported to occur in nanostructured materials, greatly improving the kinetics for hydrogen absorption and desorption [35–38]. It has been reported that nanoparticles exhibit dilated lattices that would result in larger interstitial volumes for hydrogen

^{*} Corresponding author. Tel.: +1 807 3438318; fax: +1 807 346 7775.
E-mail address: aicheng.chen@lakeheadu.ca (A. Chen).

¹ ISE member.

storage and better storage characteristics [6,17]. The characteristic hydrogen diffusion is automatically reduced due to the dilation of the lattice, leading to faster kinetics for hydrogen absorption and desorption [39,40].

Although palladium and silver have been widely used in electrochemical studies as electrodes, little attention has been directed to the synthesis and study of nanostructured palladium and silver alloys [41–44]. The relative low cost and strong structural properties of silver make it an attractive material to combine with palladium for hydrogen purification and storage. In the present study, for the first time, nanoporous Pd–Ag alloys with different amounts of Ag, varied from 0 to 40 at.%, were synthesized using a facile hydrothermal method. The behaviour and characteristics of hydrogen absorption of the nanoporous Pd–Ag alloys were studied and compared with the pure nanoporous Pd. The effects of sweep rate, electrode potential, and composition of Pd–Ag on hydrogen sorption have been systematically evaluated. Pd–Ag alloy is the most commonly used material for hydrogen extraction in industry [12]. The nanoporous Pd–Ag alloys fabricated in this study can be treated as a model system for other hydrogen sorbing materials; the knowledge gained from the present study provides insights in the design of efficient Pd-based catalysts for hydrogen purification and storage.

2. Experimental

2.1. Materials

Ammonium formate (Aldrich, 99.99%) and ethylene glycol were used as the reducing agent. Pd(NO₃)₂·xH₂O (Aldrich) and AgNO₃ (Baker) were used to prepare precursor solutions for the synthesis of the Pd–Ag nanostructures. Pure water (18.2 MΩ cm) was obtained from a Nanopure Diamond® water purification system. All other chemicals were of reagent grade.

2.2. Synthesis of Pd–Ag nanostructures

A series of Pd–Ag nanostructures with different compositions of Ag ranging from 0 to 40 at.% were directly grown onto Ti substrates using a hydrothermal method [45,46]. Ti plates (99.2%, 1.25 cm × 0.80 cm × 0.5 mm) were washed by sonication in acetone followed by pure water (18.2 MΩ cm), then etched in an 18 wt% HCl solution at 85 °C for 30 min, and finally rinsed with pure water. To fabricate the Pd–Ag nanostructures, the pre-etched Ti plates were placed in Teflon vessels containing 10 ml of an aqueous mixture of inorganic metal precursors and the reducing agent; and then the containers were heated at 180 °C for 2 h. In all cases, the amounts of the reducing agent of ammonium formate and ethylene glycol added were kept constant at 10 mM and 2.5 M, respectively. Varying amounts of the Pd(NO₃)₂·xH₂O and AgNO₃ precursors were added to obtain the desired ratio of Pd to Ag. After cooling to room temperature, the Pd–Ag coated Ti plates were finally dried in a vacuum oven at 40 °C.

2.3. Surface morphology and composition of Pd–Ag nanostructures

Following the electrode preparation, the surface morphology and composition of the coatings were characterized using a JEOL 5900LV scanning electron microscope (SEM) and X-ray energy dispersive spectrometry (EDS). The concentrations of silver and palladium in the solution after the hydrothermal reduction process were also analyzed with inductively coupled plasma (ICP). The X-ray diffraction (XRD) patterns were recorded on a PW 1050-3710 diffractometer using a Cu Kα (λ = 1.5405 Å) radiation source. X-ray

photoelectron spectra were collected using a Thermo Scientific K-Alpha XPS spectrometer. All the samples were run at a take-off angle (relative to the surface) of 90°. A monochromatic Al Kα X-ray source was used, with a spot area of 400 μm. Charge compensation was provided and the position of the energy scale was adjusted to place the main C 1s feature (C–C) at 284.6 eV. All data processing was performed using XPSpeak software.

2.4. Electrochemical study of nanoporous Pd–Ag alloys

A VoltaLab PGZ402 potentiostat was used in this work. All experiments were conducted in 0.1 M HClO₄ solution, deoxygenated by the continuous passage of ultra-pure Ar gas either into the electrolyte before electrochemical measurements or over the top of the electrolyte during electrochemical measurements. A three-electrode cell was used with a saturated calomel electrode (SCE) connected to the cell through a salt bridge as the reference electrode, a Pt wire coil as the counter electrode and the prepared Ti/Pd–Ag alloys (1 cm²) as the working electrodes. At the beginning of the absorption experiments, each of the Pd–Ag electrodes was cycled continuously through the potential region of hydrogen adsorption and absorption until an invariant voltammogram was obtained on further scanning. Data acquisition and analysis were performed using VoltMaster 4 software. All the experiments were carried out at room temperature, 22 ± 2 °C.

3. Results and discussion

3.1. Surface morphology, composition, and structure of the prepared Pd–Ag electrodes

The surface morphology of the synthesized Pd–Ag alloys was examined by SEM at a magnification of 15,000. Fig. 1a presents a typical SEM image of the Pd–Ag15% sample. All the Pd and Pd–Ag samples fabricated in this study possess nanoporous structures, similar to the Pd–Ag15% sample (Fig. 1a), consisting of irregular pores ranging from several to hundreds of nanometers in diameter. It is expected that the porous structures possess a high surface area, which is desirable for hydrogen sorption and storage. The EDS spectra of the seven nanoporous samples (pure Pd, Pd–Ag10%, Pd–Ag15%, Pd–Ag20%, Pd–Ag25%, Pd–Ag30% and Pd–Ag40%) are presented in Fig. 1b. The peaks marked by a star are derived from the Ti substrates. Two Pd peaks and two Ag peaks are observed for all the nanoporous Pd–Ag samples. As expected, the intensity of the Ag peaks progressively increases from Pd–Ag10% to Pd–Ag40%. Quantitative analysis of these EDS spectra shows that the compositions of all the Pd–Ag samples are consistent with the compositions of the Pd and Ag precursors initially added to the hydrothermal vessels. This is further confirmed by our ICP analysis. Table 1 displays the ICP results for the amount of precursors remaining in solution (i.e. not reduced) after the hydrothermal reduction. These experimental results demonstrate that the reduction agents chosen in this study can effectively reduce the Pd²⁺ and Ag⁺ precursors under the hydrothermal condition and that the composition of the formed nanoporous Pd–Ag alloy can be easily controlled using this proposed new method.

X-ray photoelectron spectroscopy (XPS) was performed to analyze the surface composition and the electronic interaction of the Pd–Ag alloys. Fig. 2 shows the high resolution XPS spectra for Pd(3d) and Ag(3d) of the sample Pd–Ag20%. The spectrum of Pd(3d) shows a doublet peaks located at a low binding energy (3d_{3/2}) at 334.4 eV and at a high binding energy (3d_{5/2}) at 339.7 eV (Fig. 2a), indicating the presence of Pd in the metallic state Pd⁰ and higher oxidation states. The binding energies of the Ag(3d_{3/2}) and Ag(3d_{5/2}) peaks (Fig. 2b) were measured at 366.5 eV and 372.4 eV, respectively.

Table 1

ICP results of the concentrations of Pd²⁺ and Ag⁺ remaining in solution after the hydrothermal reductions. Initial concentrations were calculated based on the amount of Pd(NO₃)₂ and AgNO₃ added to the hydrothermal vessels.

Sample	Pd (initial)/ppm	Pd (final)/ppm	Ag (initial)/ppm	Ag (final)/ppm	Molar ratio Pd:Ag
Pd	532.10	0.02	0.00	0.00	100:0
PdAg10%	478.89	0.06	53.93	0.00	90:10
PdAg15%	452.29	0.03	80.90	0.00	85:15
PdAg20%	425.68	0.18	107.87	0.03	80:20
PdAg25%	399.08	0.03	134.84	0.02	75:25
PdAg30%	372.47	0.13	161.80	0.00	70:30
PdAg40%	319.26	0.04	215.74	0.11	60:40

Using the area of the fitted curves for the Pd and Ag in both the metallic and the higher oxidation states, the ratio of metal/metal oxide was calculated. It was found that 92% of the Pd and 97% of the Ag were in their metallic states, further showing that the hydrothermal method employed in this study was efficient for the preparation of nanoporous Pd–Ag alloys. The actual atomic composition of Ag was also estimated based on the area under the peaks to be 17.74%, which is close to the nominal Pd:Ag ratio of 80:20.

X-ray diffraction was used to characterize the phase structure of the samples. Fig. 3a presents the XRD patterns of the nanoporous Pd and Pd–Ag samples, consistent with a face centered-cubic (fcc) unit cell. The 2θ values of 40.02°, 46.56°, 68.04° and 82.05° for the nanoporous Pd can be indexed to the diffractions of the (1 1 1), (2 0 0), (2 2 0) and (3 1 1) planes of Pd, respectively (JCPDS file no.

46-1043). The absence of Ag peaks in the XRD patterns of the nanoporous Pd–Ag samples suggests that there was no Pd and Ag crystalline metal phase separation and that Pd–Ag bimetallic alloyed structures were formed. In addition, all the peaks slightly shifted to a lower angle position due to the incorporation of increasing amounts of the larger Ag atoms into the Pd fcc lattice, indicating that the lattices in the nanoporous Pd–Ag were expanded. The fcc lattice parameter can be calculated from the diffraction peak positions. In the XRD patterns the (2 2 0) peak was used to calculate the lattice parameter a using the following equation [47]:

$$a = \frac{\sqrt{2}\lambda_{K\alpha}}{\sin \theta_{\max}} \quad (1)$$

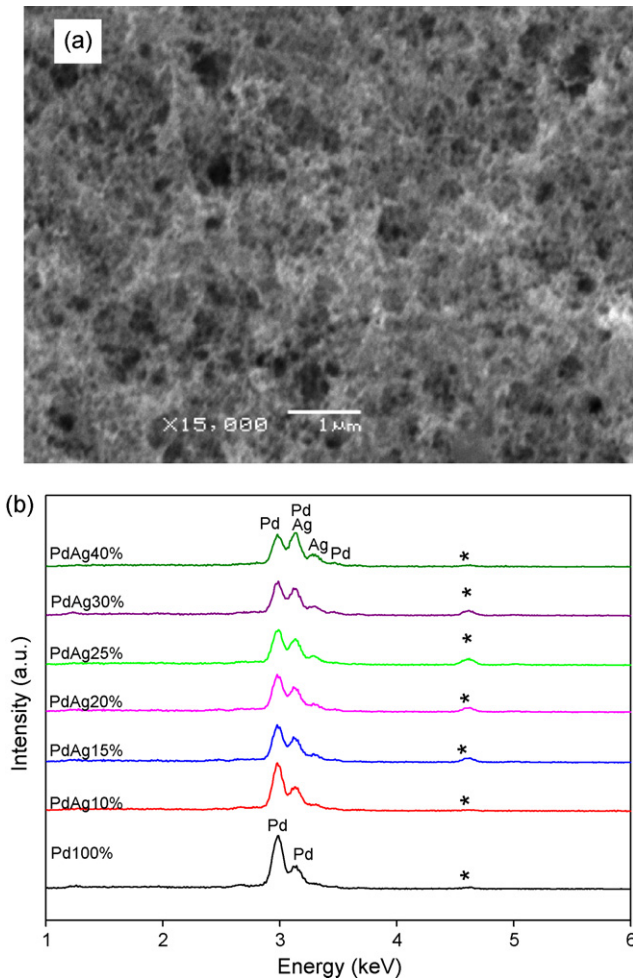


Fig. 1. (a) Typical SEM image at 15,000× magnification of the Pd–Ag surfaces with normalized atomic ratios of Pd/Ag of 85:15; (b) the EDS spectra of the nanoporous Pd and Pd–Ag alloys. The peaks labelled with * are derived from the Ti substrate.

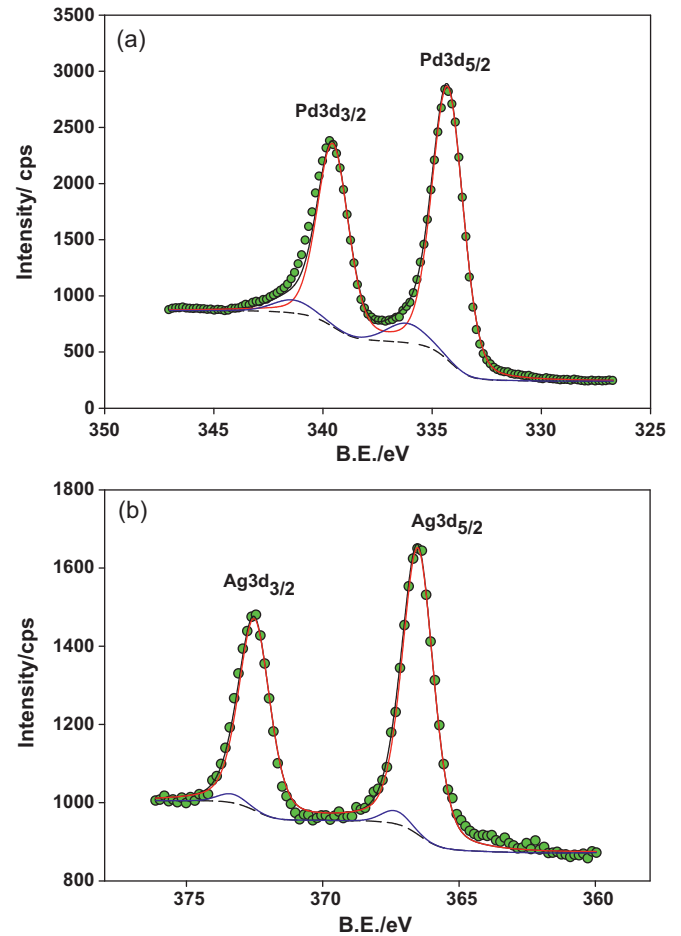


Fig. 2. XPS spectra of the Pd(3d) (a) and Ag(3d) (b) regions for the Pd–Ag20% sample. The green dots, dashed lines, and red, blue, and black solid lines represent the raw data, baseline, individual components (zero and high oxidation states) and total fit, respectively. (For interpretation of the references to color in this figure legend, the reader is referred to the web version of this article.)

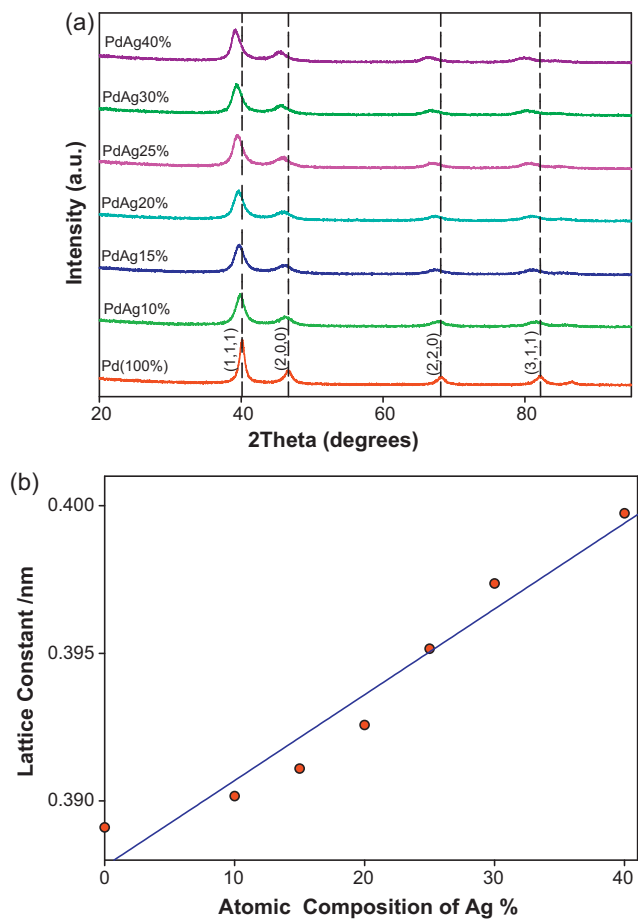


Fig. 3. (a) XRD patterns of the prepared Pd and PdAg films; (b) Vegard's plot showing the dependence of the fcc lattice constant calculated from the (2 2 0) peaks of each XRD pattern in (a) using Eq. (1) on the normalized atomic composition of Ag.

where a is the lattice constant, λ is the wavelength of X-ray radiation (Cu $K\alpha = 0.15405$ nm), and θ is the location of the (2 2 0) peak in radians. A plot of the lattice constant versus the normalized atomic composition of Ag of the nanoporous Pd–Ag alloys (Vegard's plot) is shown in Fig. 3b. The lattice constant of the Pd–Ag alloys linearly increases with the increase of the Ag component. The lattice constant of the nanoporous Pd is 0.389 nm, which increases to 0.400 nm for the Pd–Ag40% sample, showing a significant dilation of the lattice constant with increasing amounts of Ag.

3.2. General cyclic voltammetric (CV) behaviour of the Pd–Ag nanostructures

For a general hydrogen electroadsorption characterization of the nanoporous Pd and Pd–Ag alloys, two cycles of the CVs in the range of -300 to 400 mV were recorded in 0.1 M perchloric acid at a scan rate of 20 mV/s; the second cycle was presented in Fig. 4. For comparison, Fig. 4 displays the CV curves of the nanoporous Pd and Pd–Ag alloys with 10, 20 and 30 at.% Ag. As the high current caused by hydrogen absorption dominates and covers the adsorption processes, it is difficult to decouple the adsorption process from the absorption process [18]. A large broad peak due to the desorption of hydrogen appears between -300 and 0.0 mV when scanning the electrode potential from -300 mV to $+400$ mV. The integrated peak intensity for the hydrogen desorption/oxidation (i.e. the discharge) significantly increased when the Ag content was increased from 0% to 20%. Further increasing the Ag amount to 30%, the hydrogen discharge decreased, showing that the amount of Ag incorporated into

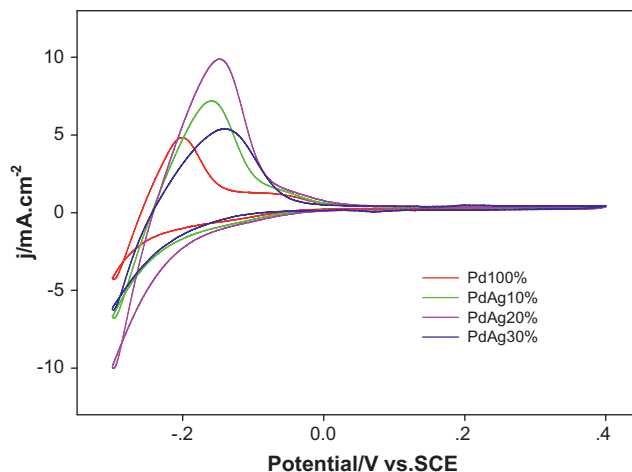


Fig. 4. Cyclic voltammograms of the PdAg electrodes recorded in 0.1 M HClO_4 at a scan rate of 20 mV/s.

Pd had a strong impact on the capacity of hydrogen sorption of the Pd–Ag nanomaterials.

3.3. Sweep rate dependence of hydrogen electroadsorption in the Pd–Ag nanostructures

To illustrate the effect of the sweep rate on the hydrogen electroadsorption, Fig. 5a presents the CV curves of the nanoporous Pd–Ag20% alloy recorded with the sweep rates varied from 5 to 50 mV/s. A well-defined hydrogen sorption peak centered at -285 mV is observed at the low sweep rate (5 mV/s). The total charge, Q_H , due to hydrogen adsorption and absorption into the Pd–Ag nanostructures versus the potential scan rate is shown in Fig. 5b. The amount of hydrogen sorbed into the nanoporous Pd–Ag alloy, calculated from the charge of the hydrogen desorption/oxidation peaks, was found to be dependent on the sweep rate used in the cyclic voltammetric experiments. Increasing the potential scan rate results in a decrease in the hydrogen discharge, showing that a low sweep rate is preferential for determining the hydrogen adsorbing/absorbing capacity of the Pd–Ag nanostructures.

3.4. Influence of the electrode potential and the composition of the Pd–Ag alloys on the capacity of hydrogen electroadsorption

The electroadsorption of hydrogen into the nanoporous Pd–Ag alloys was further examined at different electrode potentials varied from -275 to -175 mV versus SCE. The potential was first held at a constant potential for a period of time; linear voltammetry was then run starting from the held potential to $+200$ mV. The effect of the time held at different potentials on the hydrogen discharge was investigated, revealing that a period of 5 min was long enough to obtain complete saturation of hydrogen into the nanoporous Pd and Pd–Ag alloys. For comparison, Fig. 6a and b presents the linear voltammograms of the nanoporous Pd and Pd–Ag20%, respectively, recorded at the scan rate of 20 mV/s after being held at each of the pre-selected potentials for 5 min. The intensity of the hydrogen desorption/oxidation peak strongly depends on the held electrode potential; the lower the potential, the larger the peak. Similar behaviour is also observed for other nanoporous Pd–Ag alloys, reflecting the fact that, under the electrochemical conditions, the amount of hydrogen sorbed into the Pd and Pd–Ag alloys is potential dependent. A lower electrode potential corresponds to a higher hydrogen pressure in gas-phase experiments [8,26]. For pure Pd, the absorption of hydrogen produces two different phases

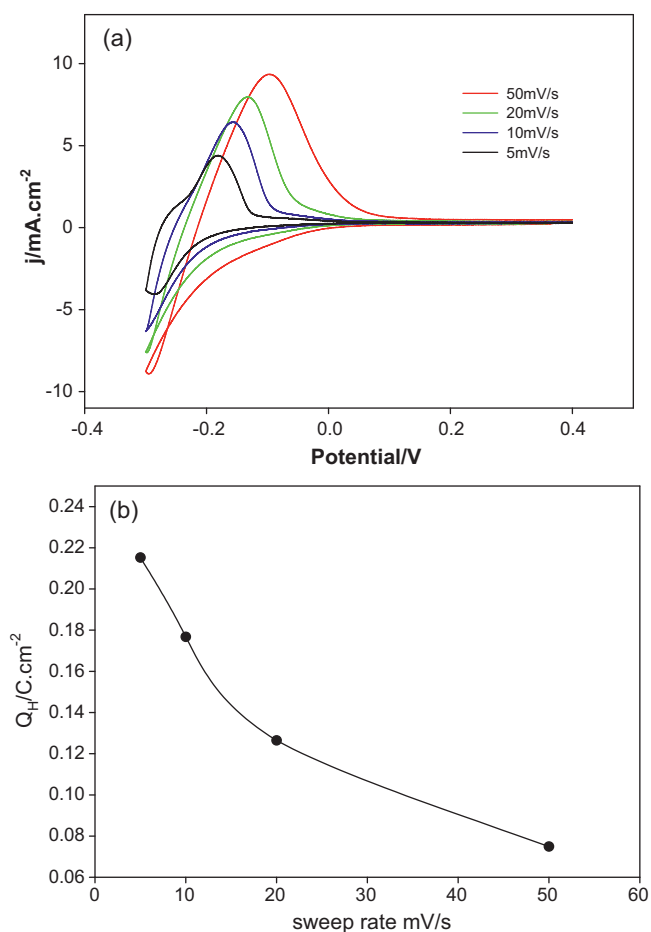


Fig. 5. (a) Cyclic voltammograms of the Pd–Ag20% electrode recorded in 0.1 M HClO₄ at various scan rates. (b) Charge due to hydrogen desorption versus sweep rate calculated by integrating the area under the anodic peaks in (a).

(α phase and β phase) [48]. At low concentrations of hydrogen, the α -phase appears, which possesses a lattice constant very similar to pure Pd. At high concentrations of hydrogen (metal hydride), the β phase forms, resulting in an increase in the lattice constant. The large expansion of the lattice constant can cause cracking of the membrane (hydrogen embrittlement). As seen in Fig. 6a, for the nanoporous Pd, a significant increase of the peak intensity is observed when the held potential was changed from -225 to -250 mV, which corresponds to the transition from the α phase to β phase hydrogen sorption. However, no sharp transition was observed for the nanoporous Pd–Ag20% (Fig. 6b). Note that the peak intensity of the nanoporous Pd–Ag20% is much higher than that of the pure nanoporous Pd when the potential was held at -225 mV.

To quantitatively examine the effect of the held potential on the capacity of the hydrogen sorption into the nanoporous Pd and Pd–Ag alloys, the total hydrogen discharge was calculated by integrating the hydrogen desorption/oxidation peak shown in Fig. 6. Fig. 7a depicts the dependence of the electrochemically measured hydrogen absorption capacity, expressed as the integrated hydrogen discharge, on the different absorption potentials for the nanoporous Pd–Ag alloys with different Ag composition varied from 0 to 40%. The plots can be divided into two sections. The potential range above -225 mV corresponds to α phase hydrogen sorption; while the potential below -225 mV leads to the β phase hydrogen sorption. Increasing the composition of Ag from 0 to 40% decreases the β phase hydrogen sorption capacity and diminishes the α to β phase transition. In contrast, increasing the composition of Ag increases the α phase hydrogen sorption capacity. After reach-

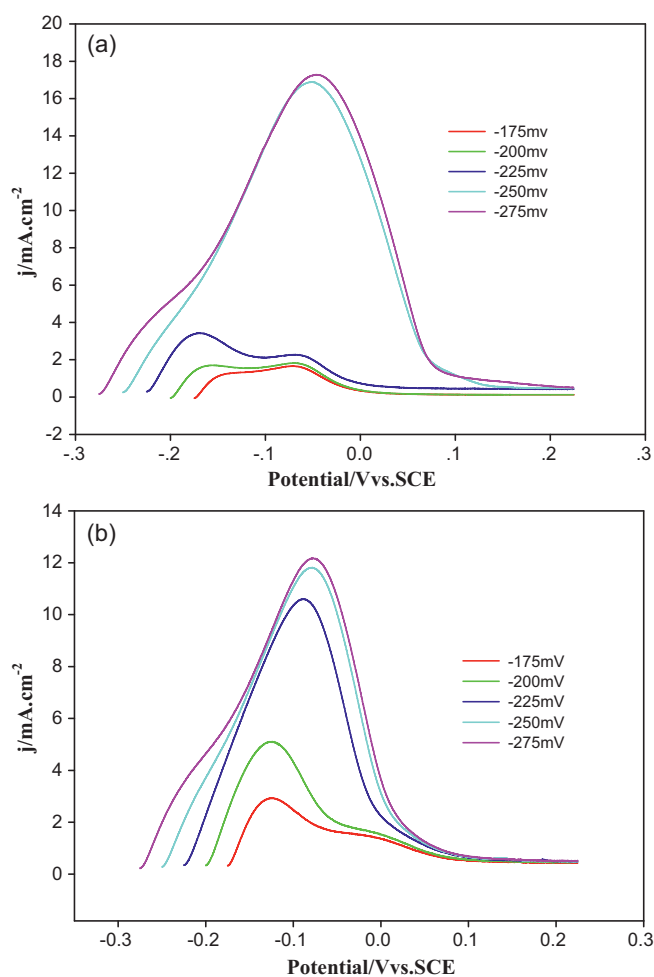


Fig. 6. Anodic sweeps of the desorption of hydrogen from (a) Pd to (b) Pd–Ag20% after holding the potential at various cathodic limits for 5 min in 0.1 M HClO₄. The scan rate was 20 mV/s.

ing the maximum capacity, further increase of the amount of Ag results in a decrease of the hydrogen sorption capacity. For comparison, Fig. 7b presents the hydrogen sorption capacity at -225 mV versus the composition of Ag of the nanoporous Pd–Ag alloys. When the Ag content is increased from 0 to 20%, the hydrogen sorption significantly increases. Further increasing the Ag content from 20% to 40%, the hydrogen sorption capacity decreased. The nanoporous Pd–Ag20% possesses the highest capacity for the α phase hydrogen sorption, which is over 4 times larger than that of the nanoporous Pd. This can be attributed to the dilation of lattice constant resulting from the incorporation of larger Ag atoms into the Pd fcc lattice as seen in Fig. 3.

3.5. Dependence of hydrogen sorption time on the electrode potential and composition of Pd–Ag

The kinetics of hydrogen sorption into the nanoporous Pd–Ag alloys was further investigated using chronoamperometry. First, the Pd–Ag electrode was held at $+200$ mV for 30 s, where neither hydrogen absorption nor adsorption occurs. The electrode potential was then stepped down to the hydrogen sorption region between -175 and -275 mV; and the corresponding chronoamperometric ($i-t$) curves were recorded (not shown here) in order to determine the time needed for a steady-state saturation of the nanoporous Pd–Ag electrodes with hydrogen. As shown in Fig. 8, the saturation time strongly depends on the composition of the nanoporous

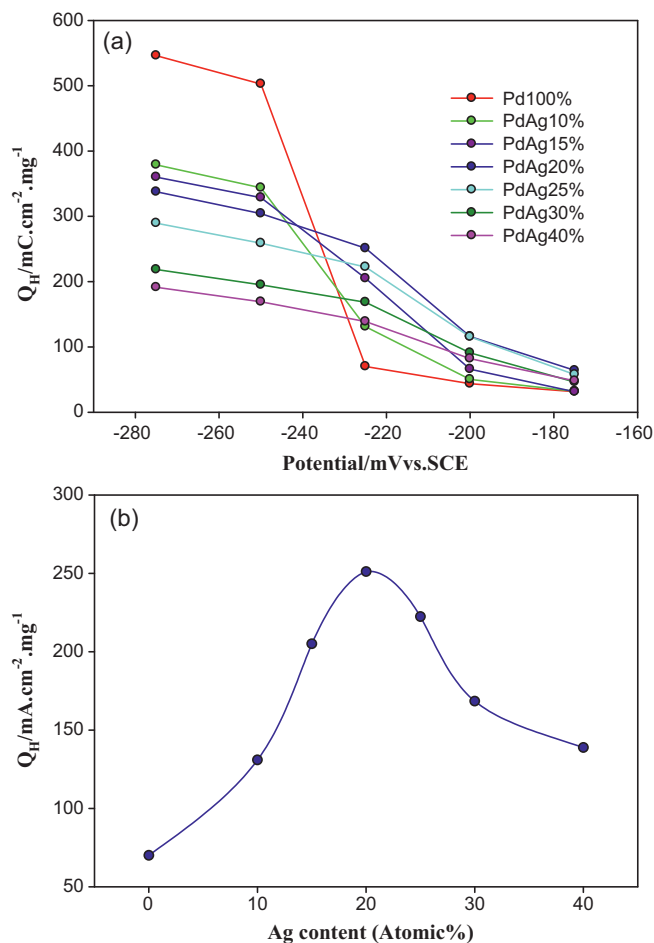


Fig. 7. (a) The overall hydrogen desorption charge, Q_H , normalized by the mass of the Pd and Pd-Ag alloys versus different potentials. (b) The overall hydrogen desorption charge, Q_H , after hydrogen electro sorption at -225 mV versus the normalized atomic composition of Ag.

PdAg alloys and the applied potential. For all the nanoporous Pd and Pd-Ag electrodes, the maximum time (t_m) required to achieve the hydrogen saturation occurs at the same potential (-250 mV), where the β phase hydrogen sorption takes place. The t_m for the nanoporous Pd is much higher than that for the nanoporous Pd-Ag electrodes. The addition of Ag dramatically lowers the maximum

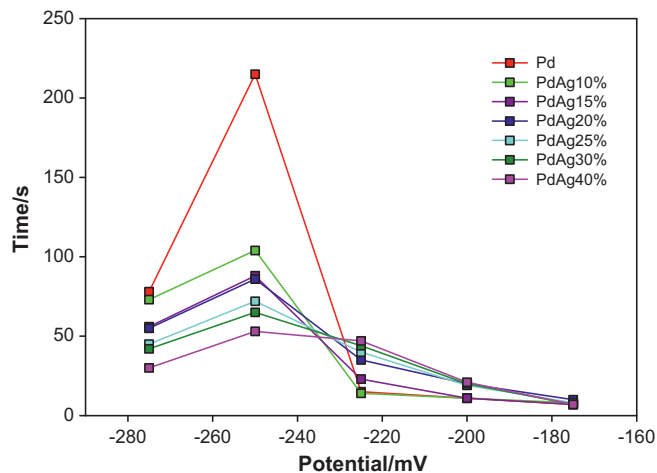


Fig. 8. The time required for obtaining steady state saturation of the electrodes with absorbed hydrogen with respect to potential.

time. The increase of the amount of Ag results in a decrease of t_m . For the nanoporous Pd, when the potential was changed from -225 to -250 mV, the time required for hydrogen saturation was increased from 15 to 215 s. This is consistent with the study of the hydrogen sorption capacity shown in Fig. 7a, where a sharp α to β phase transition was observed at -250 mV. The above results indicate that the α to β phase transition is the rate determining step and that the addition of Ag not only increases the α phase hydrogen sorption capacity, but also improves the kinetics of hydrogen sorption.

4. Conclusions

In this study, we have successfully synthesized nanoporous Pd-Ag alloys with the Ag content varied from 0 to 40% using a facile hydrothermal method. The method is very effective and can easily control the composition of the formed Pd-Ag nanostructures. Our XRD analysis shows that the lattice constant of the nanoporous Pd-Ag alloys increases with the increase of the amount of Ag. Electrochemical methods have been employed to systematically study the fabricated nanoporous Pd-Ag electrodes, showing that the hydrogen sorption into the nanoporous Pd-Ag alloys strongly depends on the composition of Pd-Ag and the applied sorption potential. Hydrogen sorption into the nanoporous Pd occurs in two distinct phases (α phase and β phase). The addition of Ag greatly increases the α phase hydrogen sorption capacity and diminishes the α - and β -phase transition due to the dilation of the lattice constant. The nanoporous Pd-Ag alloy with 20% silver content possesses the highest capacity for the α phase hydrogen sorption at -225 mV, which is over 4 times higher than the pure nanoporous Pd. Our study has also shown that the phase transition is the rate limiting step in the hydrogen absorption process and, therefore, with the addition of Ag, the kinetics is much faster. The combination of the enhanced α phase hydrogen sorption capacity and diminishing of the α - and β -phase transition makes the nanoporous Pd-Ag alloys attractive for hydrogen selective membranes and hydrogen dissociation catalysts.

Acknowledgements

This work was supported by a Discovery Grant from the Natural Sciences and Engineering Research Council of Canada (NSERC). A. Chen acknowledges NSERC and the Canada Foundation of Innovation (CFI) for the Canada Research Chair Award in Material and Environmental Chemistry. We also thank the Surface Interface Ontario/Chemical Engineering & Applied Chemistry at the University of Toronto for carrying out the XPS analysis of the Pd-Ag samples.

References

- [1] J.A. Turner, *Science* 305 (2004) 972.
- [2] E. Reguera, *Int. J. Hydrogen Energy* 34 (2009) 9163.
- [3] A. Hamaed, T.K.A. Hoang, M. Trudeau, D.M. Antonelli, *J. Organomet. Chem.* 694 (2009) 2793.
- [4] Q. Peng, G. Chen, H. Mizuseki, Y. Kawazoe, *J. Chem. Phys.* 131 (2009) 214505.
- [5] M. Lukaszewski, K. Kusmierczyk, J. Kotowski, H. Siwek, A. Czerwinski, *J. Solid State Electrochem.* 7 (2003) 69.
- [6] H. Kobayashi, M. Yarnauchi, H. Kitagawa, Y. Kubota, K. Kato, M. Takata, *J. Am. Chem. Soc.* 130 (2008) 1828.
- [7] C. Amorim, M.A. Keane, *J. Colloid Interface Sci.* 322 (2008) 196.
- [8] N. Comisso, A. De Ninno, E. Del Giudice, G. Mengoli, P. Soldan, *Electrochim. Acta* 49 (2004) 1379.
- [9] Y. Li, Y.T. Cheng, *Int. J. Hydrogen Energy* 21 (1996) 281.
- [10] Y. Chen, C. Sequeira, T. Allen, C.P. Chen, *J. Alloys Compd.* 404 (2005) 661.
- [11] O. Friedrichs, L. Kolodziejczyk, J.C. Sanchez-Lopez, A. Fernandez, L. Lyubenova, D. Zander, U. Koster, K.F. Aguey-Zinsou, T. Klassen, R. Bormann, *J. Alloys Compd.* 463 (2008) 539.
- [12] Y.G. Sun, Z.L. Tao, J. Chen, T. Herricks, Y.N. Xia, *J. Am. Chem. Soc.* 126 (2004) 5940.
- [13] M. Yamauchi, R. Ikeda, H. Kitagawa, M. Takata, *J. Phys. Chem. C* 112 (2008) 3294.

- [14] A. Czerwinski, I. Kiersztyn, M. Grden, J. Czaplá, J. Electroanal. Chem. 471 (1999) 190.
- [15] F. Kadirgan, A.M. Kannan, T. Atilan, S. Beyhan, S.S. Ozenler, S. Suzer, A. Yorur, *Int. J. Hydrogen Energy* 34 (2009) 9450.
- [16] M. Grden, A. Piascik, Z. Koczorowski, A. Czerwinski, J. Electroanal. Chem. 532 (2002) 35.
- [17] I. Avila-Garcia, M. Plata-Torres, M.A. Dominguez-Crespo, C. Ramirez-Rodriguez, E.M. Arce-Estrada, J. Alloys Compd. 434 (2007) 764.
- [18] C. Gabrielli, P.P. Grand, A. Lasia, H. Perrot, J. Electrochem. Soc. 151 (2004) A1925.
- [19] C. Gabrielli, P.P. Grand, A. Lasia, H. Perrot, J. Electrochem. Soc. 151 (2004) A1937.
- [20] M.H. Martin, A. Lasia, *Electrochim. Acta* 53 (2008) 6317.
- [21] A. Lasia, J. Electroanal. Chem. 593 (2006) 159.
- [22] H. Li, H.Y. Xu, W.Z. Li, J. Membr. Sci. 324 (2008) 44.
- [23] A. Zurowski, M. Lukaszewski, A. Czerwinski, *Electrochim. Acta* 53 (2008) 7812.
- [24] M. Słojewski, J. Kowalska, R. Jurczakowski, J. Phys. Chem. C 113 (2009) 3707.
- [25] M. Grden, A. Czerwinski, J. Golimowski, E. Bulska, B. Krasnodebska-Ostrega, R. Marassi, S. Zamponi, J. Electroanal. Chem. 460 (1999) 30.
- [26] A. Zurowski, M. Lukaszewski, A. Czerwinski, *Electrochim. Acta* 51 (2006) 3112.
- [27] E.L. Foletto, J.V.W. Da Silveira, S.L. Jahn, *Latin Am. Appl. Res.* 38 (2008) 79.
- [28] B.D. Adams, G.S. Wu, S. Nigrio, A. Chen, J. Am. Chem. Soc. 131 (2009) 6930.
- [29] B.D. Adams, C.K. Ostrom, A. Chen, *Langmuir* 26 (2010) 7632.
- [30] M. Łukaszewski, K. Klimek, A. Czerwiński, J. Electroanal. Chem. 637 (2009) 13.
- [31] T. Kuji, Y. Matsumura, H. Uchida, T. Aizawa, J. Alloys Compd. 330 (2002) 718.
- [32] X.C. Chen, Y.Q. Hou, H. Wang, Y. Cao, J.H. He, J. Phys. Chem. C 112 (2008) 8172.
- [33] M. Polanski, J. Bystrzycki, J. Alloys Compd. 486 (2009) 697.
- [34] H.-P. Liang, N.S. Lawrence, T.G.J. Jones, C.E. Banks, C. Ducati, J. Am. Chem. Soc. 129 (2007) 6068.
- [35] X.H. Tan, C.T. Harrower, B.S. Amirkhiz, D. Mitlin, *Int. J. Hydrogen Energy* 34 (2009) 7741.
- [36] H. Barlag, L. Opara, H. Zuchner, J. Alloys Compd. 330 (2002) 434.
- [37] S. Heinze, B. Vuillemin, J.C. Colson, P. Giroux, D. Leterq, *Solid State Ion.* 122 (1999) 51.
- [38] T.K. Nielsen, K. Manickam, M. Hirscher, F. Besenbacher, T.R. Jensen, *ACS Nano* 3 (2009) 3521.
- [39] S. Kishore, J.A. Nelson, J.H. Adair, P.C. Eklund, J. Alloys Compd. 389 (2005) 234.
- [40] M. Yamauchi, H. Kobayashi, H. Kitagawa, *ChemPhysChem* 10 (2009) 2566.
- [41] V.R.R. Medicherla, W. Drube, *Appl. Surf. Sci.* 256 (2009) 376.
- [42] W.H. Lin, H.F. Chang, *Surf. Coat. Technol.* 194 (2005) 157.
- [43] A. Kibria, Y. Sakamoto, *Int. J. Hydrogen Energy* 25 (2000) 853.
- [44] L.S. McLeod, F.L. Degertekin, A.G. Fedorov, J. Membr. Sci. 341 (2009) 225.
- [45] J.P. Wang, D.F. Thomas, A. Chen, *Chem. Commun.* (2008) 5010.
- [46] J. Wang, P. Holt-Hindle, D. MacDonald, D.F. Thomas, A. Chen, *Electrochim. Acta* 53 (2008) 6944.
- [47] Y.J. Huang, X.C. Zhou, J.H. Liao, C.P. Liu, T.H. Lu, W. Xing, *Electrochem. Commun.* 10 (2008) 1155.
- [48] D.G. Narehood, S. Kishore, H. Goto, J.H. Adair, J.A. Nelson, H.R. Gutiérrez, P.C. Eklund, *Int. J. Hydrogen Energy* 34 (2009) 952.